Triggers of Full-Length Tau Aggregation: A Role for Partially Folded Intermediates†

Carmen N. Chirita,‡,§ Erin E. Congdon,‡,|| Haishan Yin,‡,⊥ and Jeff Kuret*,#

Biophysics, Neuroscience, and Biochemistry Graduate Programs, The Ohio State University, and Department of Molecular and Cellular Biochemistry, The Ohio State University College of Medicine and Public Health, Columbus, Ohio 43210

Received January 3, 2005; Revised Manuscript Received February 22, 2005

ABSTRACT: Alzheimer's disease is characterized in part by the accumulation of full-length tau proteins into intracellular filamentous inclusions. To clarify the events that trigger lesion formation, the aggregation of recombinant full-length four-repeat tau (htau40) was examined in vitro under near-physiological conditions using transmission electron microscopy and spectroscopy methods. In the absence of exogenous inducers, tau protein behaved as an assembly-incompetent monomer with little tertiary structure. The addition of anionic inducers led to fibrillization with nucleation-dependent kinetics. On the basis of circular dichroism spectroscopy and reactivity with thioflavin S and 8-anilino-1-naphthalenesulfonic acid fluorescent probes, the inducer stabilized a monomeric species with the folding characteristics of a premolten globule state. Planar aromatic dyes capable of binding the intermediate state with high affinity were also capable of triggering fibrillization in the absence of other inducers. Dye-mediated aggregation was characterized by concentration-dependent decreases in lag time, indicating increased nucleation rates, and submicromolar critical concentrations, indicating a final equilibrium that favored the filamentous state. The data suggest that the rate-limiting barrier for filament formation from full-length tau is conformational and that the aggregation reaction is triggered by environmental conditions that stabilize assembly-competent conformations.

Tau is a microtubule-associated protein implicated in the progression of AD[1] and other tauopathic neurodegenerative diseases (*1*). It purifies from normal brain tissue as an ensemble of alternative splice products with monomeric quaternary structure (*2*). In disease, however, tau protein accumulates in lesions composed of fibrillar aggregates displaying the cross-β-sheet diffraction pattern of "amyloid" (*3*). In vitro, tau can be induced to assemble with sigmoidal kinetics consistent with a nucleation-dependent process (*4*, *5*). This behavior is typically ascribed to the requirement for a necessary but scarce species in the reaction pathway termed the "nucleus" (*6*). Once formed, however, subsequent lengthening of the nascent filament by stepwise addition of protomeric species is energetically favorable and follows in a reaction termed elongation. The favorable elongation reaction relative to the less favorable nucleation reaction results in the characteristic features of this mechanism, including a preequilibrium phase characterized by a time lag during which nucleation proceeds, the existence of a critical protomer concentration, below which filament formation is not supported, and seeding behavior, whereby the addition of preformed nuclei or filaments surmounts the energy barrier of nucleation. Experience with recombinant tau constructs suggests, however, that classic nucleation−elongation theory as elaborated for spontaneous self-association (i.e., homogeneous nucleation) is insufficient to completely account for the aggregation behavior of tau. For example, recombinant full-length tau produced in vitro or through expression in situ does not spontaneously assemble as predicted by theory, even at high levels of supersaturation (*7*−*9*). Moreover, the predicted seeding behavior is inefficient in the absence of exogenous fibrillization promoters (*9*, *10*).

These data suggest that molecular events in addition to those underlying classic nucleation−elongation behavior are responsible for triggering the fibrillization of full-length tau isoforms. Because tau is posttranslationally modified in disease, abnormal phosphorylation, glycation, and/or oxidation reactions have all been suggested to play triggering roles. Experience with phosphorylation mimicry mutants in the context of purified recombinant tau preparations indicates, however, that although modifications can promote fibrillization, the mechanism is limited to enhancement of the elongation reaction through lowering of the critical concentration for assembly (*11*). Similar results were found for glycated recombinant tau preparations (*11*). Moreover, oxidation of tau into disulfide-bonded dimers can accelerate fibrillization without triggering it (*12*), and both N- and C-terminal proteolyic truncations are later stage events in disease temporally unrelated to the triggering reaction (*13*).

† This work was supported by grants from the National Institutes of Health (AG14452) and the Alzheimer's Association (RG2-29-076).

* To whom correspondence should be addressed at the OSU Center for Biotechnology. Tel: (614) 688-5899. Fax: (614) 292-5379. E-mail: kuret.3@osu.edu.

‡ These authors contributed equally to this work.

§ Biophysics Program.

|| Neuroscience Program.

⊥ Biochemistry Program.

Department of Molecular and Cellular Biochemistry.

[1] Abbreviations: AA, arachidonic acid; AD, Alzheimer's disease; ANS, 8-anilino-1-naphthalenesulfonic acid; EM, electron microscopy; ThS, thioflavin S; TR, thiazin red.

10.1021/bi0500123 CCC: $30.25
Published on Web 03/25/2005

In fact, the ultrastructure of tau filaments in AD tissue suggests that the trigger may not involve spontaneous self-association at all. In end stage disease, individual PHFs appear in endwise association with membranes, consistent with surface-mediated nucleation and unidirectional extension from stable tau−membrane complexes (*14*). These data are consistent with a heterogeneous nucleation mechanism, where association of tau with other intracellular components triggers aggregation. This reaction can be mimicked in vitro by contacting purified preparations of full-length recombinant tau protein with polyanions or anionic micelles, vesicles, or microspheres, with fibrillization proceeding over a period of hours (*5*, *15*, *16*). Immediately after contact, and well before filament formation, species of tau form that can be detected by ThS, a noncovalent probe of β-sheet structure (*5*). We have termed these species "intermediates", because of the timing of their appearance during the reaction time course, and have proposed that they are the true substrates for the nucleation reaction. This interpretation predicts that tau fibrillization is triggered by conditions that support the adoption of assembly-competent conformations.

Here we test this hypothesis using full-length recombinant tau protein and anionic inducers of assembly. The data indicate that the stabilization of an intermediate folding state characterized by increased β-sheet structure is sufficient to trigger the fibrillization of full-length tau protein.

EXPERIMENTAL PROCEDURES

Materials. Recombinant His-tagged htau40 was prepared as described previously (*17*, *18*). AA (Cayman Chemicals, Ann Arbor, MI) was dissolved in ethanol (333 mM) and stored at −80 °C until used. Glutaraldehyde, uranyl acetate, and 300 mesh carbon-coated copper grids were from Electron Microscopy Sciences (Fort Washington, PA). Stock solutions of thiazin red (TCI America, Portland, OR) and ThS (Sigma, St. Louis, MO) were prepared in water, whereas Congo Red (City Chemical, West Haven, CT) and ANS (Sigma, St. Louis, MO) were prepared in DMSO and ethanol, respectively. Carboxylate-conjugated polystyrene microspheres (90 nm diameter, molecular area = 12 Å^2/eq) were from Bangs Laboratories, Inc. (Fishers, IN).

Fibrillization Assays. Under standard conditions, htau40 was incubated without agitation in assembly buffer (10 mM HEPES, pH 7.4, 100 mM NaCl, 5 mM dithiothreitol) at 37 °C for up to 24 h in the presence or absence of fibrillization inducers (AA, carboxylate-modified microspheres, ThS, Congo Red, thiazin red, or ANS). For analysis by EM, aliquots were removed, treated with 2% glutaraldehyde (final concentration), mounted on Formvar/carbon-coated 300 mesh grids, and negatively stained with 2% uranyl acetate as described previously (*9*, *16*). Random images were viewed in a Phillips CM 12 transmission electron microscope operated at 65 kV, captured on film at 8000−60000-fold magnification, digitized, and imported into Optimas 6.5.1 for quantification of filament lengths and numbers (*9*). Individual filaments ≥50 nm in length were counted manually.

ThS Fluorescence Measurements. Tau was aggregated at 37 °C as described above except that the reactions contained 10 μM ThS. Resultant changes in fluorescence were monitored at λ_{ex} = 440 nm and λ_{em} = 495 nm in a FlexStation plate reader (Molecular Devices, Sunnyvale, CA) operated at sensitivity 10, high PMT using black-matrix, clear-bottom 96-well isoplates (Wallac, Turku, Finland) sealed with transparent foil (NUNC, Denmark).

Circular Dichroism. Samples were prepared for CD analysis by desalting (Bio-Rad Econo-Pac 10DG column) into 100 mM $NaClO_4$ and 10 mM H_3BO_3, pH 7.4. These buffer components were employed because of their transparency at far-UV wavelengths (*19*). Spectra were collected (186−260 nm) at 25 °C with an AVIV model 202 CD spectrometer and a quartz cuvette with 1 mm path length. Four repetitive scans (4 s integration time, 1 nm step size, and 1 nm bandwidth) were recorded, averaged, and corrected for buffer-only blank without additional filtering or smoothing. Raw CD signals (in millidegrees) were converted to mean residue molar ellipticity $[\theta]_M$ (with units of deg·cm^2/dmol) using the formula $[\theta]_M = [\theta]_{obs}/(10lcn)$, where $[\theta]_{obs}$ is the observed ellipticity in millidegrees, l is the path length in centimeters, c is the molar concentration of protein, and n is the number of residues in the protein (*20*). Secondary structure compositions of α-helix (normal and distorted), β-strand (normal and distorted), turns, and random coil were estimated from net spectra using CONTIN/LL (*21*), CDSSTR (*22*), and SELCON3 (23) algorithms. Resultant estimates were then averaged and presented ± SD (*24*).

Hydrodynamic Analysis. Analytical size-exclusion chromatography was performed (4 °C) on a 24 mL (10 × 300 mm) Superose 6 10/300GL column equilibrated with 10 mM HEPES, pH 7.0, and 100 mM NaCl buffer and operated at 0.5 mL/min. Standards (*25*) included thyroglobulin (8.0 nm), equine apoferritin (6.2 nm), yeast alcohol dehydrogenase (4.6 nm), and bovine serum albumin (3.6 nm). Hydrodynamic radii were estimated from partition coefficients as described previously (*26*).

Velocity sedimentation measurements were performed in linear 4−20% sucrose gradients containing 10 mM HEPES, pH 7.4, and 150 mM NaCl. Standards included bovine serum albumin (4.3 S), bovine erythrocyte carbonic anhydrase (3.2 S), myoglobin (1.9 S), and cytochrome *c* (1.6 S). After centrifugation (200000*g* for 20 h at 4 °C), gradients were fractionated and sedimentation coefficients were estimated as described previously (*26*). Native molecular mass was calculated from hydrodynamic parameters as described previously (*27*) using a partial specific volume calculated from the tau amino acid sequence (*28*). Theoretical hydrodynamic radii for tau in native, molten globule, premolten globule, random coil, and denatured states were calculated from molecular mass using the empirical equations deduced by Tcherkasskaya et al. (*29*). Observed (i.e., apparent) frictional ratios $(f/f_0)_{obs}$ were calculated from hydrodynamic radii (r_{hyd}) by the equation (*27*):

$$(f/f_0)_{obs} = r_{hyd}/[(3\nu M/4\pi N)^{1/3}] \quad (1)$$

where ν is the partial specific volume calculated as described above, M is the molecular mass, and N is Avogadro's number.

Analytical Methods. Sigmoidal reaction progress curves were fit to a three-parameter Gompertz function as described previously (*4*). Lag times, defined as the time when the tangent to the point of maximum polymerization rate

Table 1: Recombinant Htau40 Physical Properties

hydrodynamic radius (nm)	5.5 ± 0.9
sedimentation coefficient ($s_{20,w}$)	2.0 ± 0.1
native molecular mass (Da)[a]	45000 ± 8000
native molecular mass (Da)[b]	47881
native structure	monomer
$(f/f_0)_{obs}$	2.32 ± 0.39
$(f/f_0)_{shape}$	1.95 ± 0.33[c]
axial ratio (prolate ellipsoid)	~19:1

[a] Estimated from hydrodynamic parameters. [b] Estimated by mass spectroscopy. [c] Corrected for hydration assuming 0.5 g of water/g of protein.

intersects the abscissa of the sigmoidal curve (*30*), were calculated from the resultant Gompertz parameters (*4*).

Hyperbolic reaction progress curves were fit to the polynomial series (*31*):

$$y = \alpha + \beta t + \gamma t^2 + ... + \zeta t^6 \quad (2)$$

where y is fluorescence intensity at time t, and the coefficient β approximates the initial velocity.

Concentration−response data were fit to a three-parameter log-normal function:

$$y = ae^{\{-0.5[\ln(x/x_o)/b]^2\}} \quad (3)$$

where y is the amount of product at ligand concentration x, a is the maximum amount of product appearing at optimal concentration x_o, and b is a constant.

Nucleation statistics were fit to a Poisson distribution:

$$P(n) = \frac{e^{-\lambda}\lambda^n}{n!} \quad (4)$$

where $P(n)$ is the probability of a microsphere randomly nucleating n filaments when the average number of filaments per microsphere is λ.

RESULTS

Recombinant Tau Protein Is an Extended Monomer in Solution. Authentic tissue-derived tau proteins are asymmetric monomers when free in solution (*2*). Conversely, it has been claimed that recombinant tau forms dimers at high concentration (*12*) in a reaction that is further favored by the presence of a poly-His tag (*32*). Dimerization has been postulated as a key prenucleation step in tau aggregation (*12*). In view of these conflicting claims, recombinant htau40 was subjected to hydrodynamic analysis using a combination of gel filtration chromatography and velocity sedimentation. Results show that, under the near-physiological buffer conditions used for fibrillization experiments, recombinant htau40 is an asymmetric monomer with hydrodynamic properties similar to those of authentic tau (compare Table 1 with ref *2*).

Empirical formulas relating hydrodynamic radius to chain length have been derived for different folding states (*29*). The utility of these equations for comparing proteins of differing chain lengths can be increased by converting hydrodynamic radii into frictional ratios $(f/f_0)_{obs}$ as described in Experimental Procedures. Comparison of the experimentally determined $(f/f_0)_{obs}$ value for recombinant poly-His-tagged human htau40 with these theoretical predictions

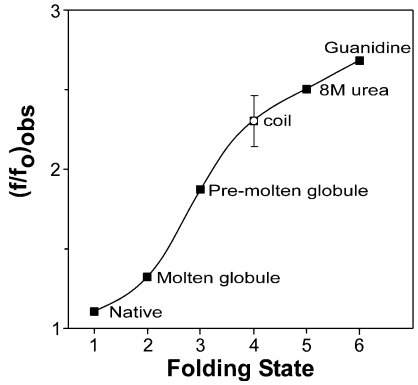

FIGURE 1: Tau protein is a monomer with random coil character. The $(f/f_0)_{obs}$ (observed frictional ratio) estimated for recombinant poly-His-tagged htau40 by hydrodynamic methods (○; Table 1) was compared to theoretical values (■) for the protein in six folding states (1, native; 2, molten globule; 3, premolten globule; 4, random coil; 5, denatured in 8 M urea; and 6, denatured in 6 M guanidine hydrochloride) calculated (by eq 1) on the basis of empirical correlations between the hydrodynamic radius and chain length (*29*). Each folding state is depicted as a category arbitrarily placed at equal intervals on the abscissa, whereas the solid line is drawn solely to aid visualization. The relative errors for calculated $(f/f_0)_{obs}$ values are reportedly ≤10% (*29*). The hydrodynamic behavior of the tau preparation used throughout this work was characteristic of a monomer in random coil state.

indicated that the preparation consists of a monomer in random coil conformational state at the start of the aggregation pathway (Figure 1), consistent with the behavior of tissue-derived porcine tau (*2*) and recombinant nontagged human htau40 (*33*).

Surface-Mediated Intermediate Formation Is First Order with Respect to Tau Concentration. Monomer progresses to polymer through an intermediate stage characterized by an ability to bind ThS, a fluorescent probe of β-sheet structure (*5*). Because ThS fluorescence appeared immediately during fibrillization lag time and also below the critical concentration of filament formation as assessed by electron microscopy and laser light scattering measurements, it was assumed to directly reflect the concentration of nonfilamentous species. To further characterize these species, the time course of ThS fluorescence resulting from incubation of monomeric htau40 in the presence of carboxylated microspheres was followed in real time. ThS fluorescence appeared immediately upon contacting the microspheres and then increased hyperbolically as a function of time (Figure 2A). In contrast, preincubation of tau with microspheres prior to addition of probe resulted in immediate formation of ThS fluorescence, whereas incubation of tau with ThS alone (at low micromolar concentration) yielded only modest fluorescence (data not shown). These data confirmed that intermediates formed after contacting the microsphere surface and were not induced by the presence of low micromolar concentrations of probe.

Previously, intermediate formation was shown to be first order with respect to microsphere concentration (*5*). To determine reaction order with respect to tau protein, the intial velocity of ThS fluorescence production was measured as a function of tau concentration. Because initial velocities were estimated during fibrillization lag time, the rate of appearance of ThS fluorescence was assumed to reflect the formation of prefibrillar species. Replots of these data in double log format revealed a slope of 0.90 ± 0.02, indicating that the appearance of ThS fluorescence is first order with respect

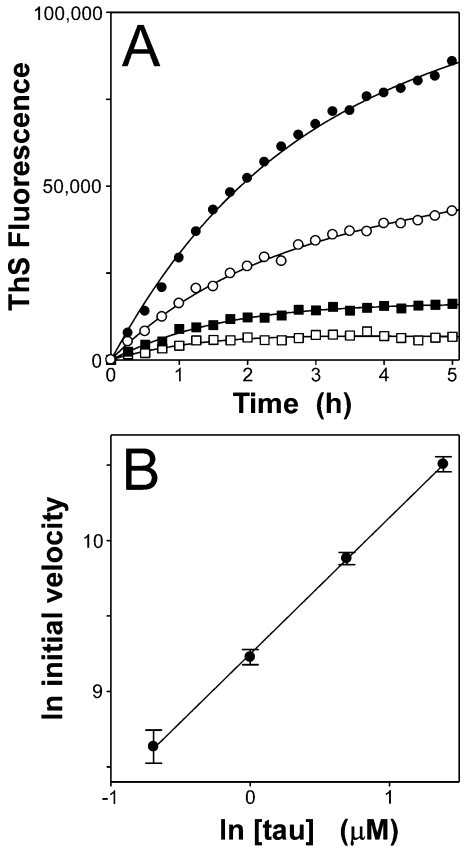

FIGURE 2: Intermediate formation is first order with respect to tau concentration. (A) The time course of ThS fluorescence formation resulting from incubation (37 °C) of htau40 at 0.5 (□), 1 (■), 2 (○), and 4 μM (●) in the presence of carboxylate-substituted polystyrene microspheres (90 nm diameter, 11.6 Å^2/eq molecular area; 124 pM) was followed by fluorescence spectroscopy. Each point represents a fluorescence measurement at time *t*, whereas solid lines represent the best fit of the data points to a sixth power polynomial series. The rate and extent of ThS fluorescence increased with increasing tau concentrations. (B) Replot of the initial velocities ± SE estimated from the progress curves shown in panel A versus tau concentration in double logarithmic format, where the line represents the best fit of the data points to a linear regression. The slope of the replot (0.90 ± 0.02) was consistent with the initial velocity of ThS signal generation being directly proportional to tau concentration under these experimental conditions.

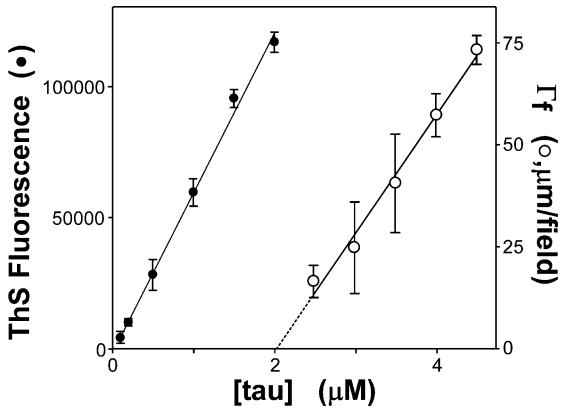

FIGURE 3: Critical concentration for tau filament and intermediate formation in the presence of anionic microspheres. Carboxylate-substituted polystyrene microspheres (90 nm diameter, 11.6 Å^2/eq molecular area; 124 pM) were incubated (24 h at 37 °C) with varying concentrations of htau40 (0−4 μM) in the presence of ThS (4 μM) and then assayed for fibrillization by EM (○) and intermediate formation by ThS fluorescence (●) assays. Each data point represents the mean ± SD of triplicate determinations whereas the solid lines represent the best fit of the data points to a linear regression (eq 2). In the case of fibrillization, the regression line intercepted the abscissa at 2.06 ± 0.10 μM htau40, indicating the existence of a critical concentration. In contrast, ThS fluorescence was detectable below the critical concentration of fibrillization, with the regression line intersecting the abscissa at the origin. Whereas fibrillization was characterized by a critical concentration, appearance of ThS fluorescence was not.

to tau protein concentration (Figure 2B). These data suggest that the intermediate corresponds to a conformation of monomer. It further suggests that aggregation of tau into supramolecular complexes occurs after intermediate formation.

Nucleation−elongation reactions are characterized by a critical concentration, above which all additional protomers incorporate into filaments (*34*). It is the highest protein monomer concentration that does not support fibrillization and, therefore, corresponds to the abscissa intercept of the tau concentration dependence curve (*35*). To determine the relationship between intermediate formation and filament critical concentration, the monomer concentration dependence of htau40 fibrillization and intermediate formation was determined in the presence of carboxylated microspheres using EM and ThS fluorescence assays, respectively. Fibrillization was directly proportional to tau concentration with an abscissa intercept of 2.06 ± 0.10 μM (Figure 3). This value is consistent with estimates made by laser light scattering methods in the presence of anionic surfactants (*4*, *11*) and indicates that the final equilibrium between filament ends and unincorporated tau is similar in the presence of diverse anionic inducers. The relationship between final ThS fluorescence intensity at equilibrium and tau concentration below the critical concentration for fibrillization also was linear under these conditions (Figure 3). In contrast to filament formation, however, the curve intersected the abscissa within one standard error of the estimate of the origin (0.03 ± 0.05 μM) (Figure 3), indicating that intermediate formation did not have a critical concentration. These data are consistent with the ThS-reactive intermediate being a monomer that does not require a minimal concentration for formation.

Intermediate Secondary Structure. The ability of the tau intermediate to bind the ThS probe suggests it contains increased β-sheet structure relative to natively unfolded recombinant starting material. To test this prediction, htau40 was incubated in the presence or absence of arachidonic acid inducer for 20 min and then subjected to circular dichroism spectroscopy. The analysis was conducted at the critical concentration and within fibrillization lag time to ensure that mature filaments did not contribute to the circular dichroism signal. In the absence of arachidonic acid, full-length htau40 yielded a CD spectrum typical of unfolded proteins, with a broad minimum of ellipticity centered at 195 nm and a shoulder at 220 nm (Figure 4A). Molar ellipticities at 200 and 222 nm were −13538 and −3236, respectively, consistent with theoretical studies showing that the coiled state can accommodate substantial local secondary structure (*36*). The presence of arachidonic acid led to an increase in the $[\theta]_{222}/[\theta]_{200}$ ratio, consistent with intermediate formation being accompanied by an increase in secondary structure and a loss in random coil (Figure 4A). The final ellipticity values at 222 and 200 nm were characteristic of the premolten

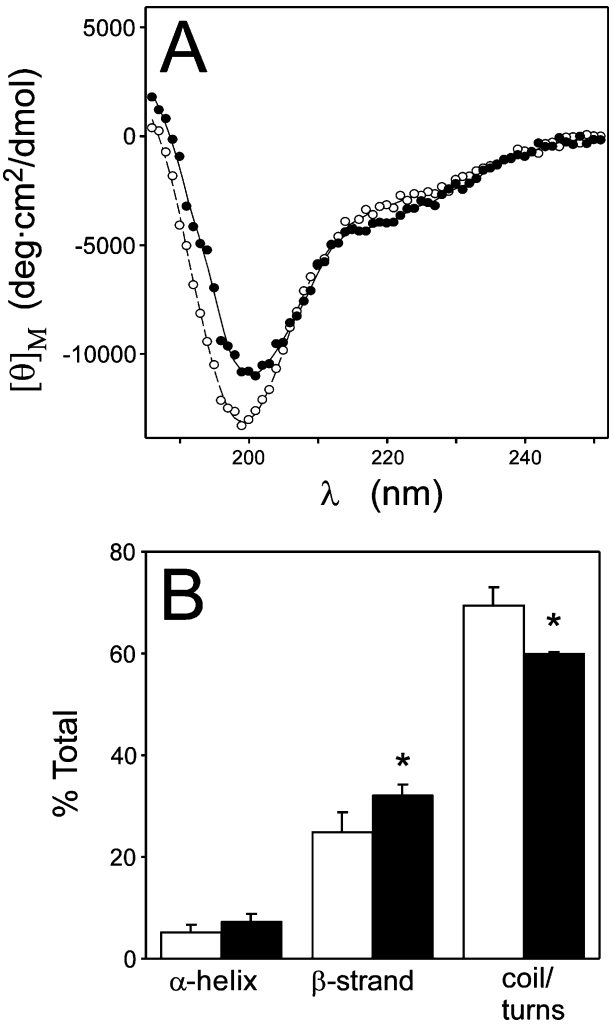

FIGURE 4: Intermediate formation is accompanied by changes in secondary structure. Htau40 (2.0 μM) was incubated (20 min at 25 °C) in 100 mM sodium perchlorate and 20 mM boric acid, pH 7.4, in the presence (●) or absence (○) of 50 μM AA inducer and then immediately subjected to far-UV CD spectroscopy (37 °C). (A) Intermediate formation was accompanied by an increase in $[\theta]_{195}$ and a decrease in $[\theta]_{220}$, consistent with the formation of secondary structure. (B) CD spectra were individually fit by CDSTTR, SELCON3, and CONTIN/LL algorithms to calculate estimates of total α-helical, β-strand, and random coil/turn conformation. The three estimates were then averaged and plotted ± SD for htau40 in the presence (black bars) or absence (white bars) of AA inducer. Intermediate formation was accompanied by increases in β-conformation and decreases in random coil/turn conformation. *, $p < 0.05$, comparing the two populations.

globule folding state (*37*). The amounts of secondary structure were estimated by fitting CD spectra to three independent algorithms as described in Experimental Procedures (Figure 4B). In the absence of inducer, htau40 adopted 5.5 ± 1.4% α-helix, 25.0 ± 3.9% β-strand, and 69.4 ± 3.6% random coil/turn conformation. These values were generally similar to those found at room temperature for bovine tau isolated without harsh heat or acid treatments (*38*). The inducer converted an additional 7.1 ± 1.2% of residues to β-conformation at the expense of random coil/turn conformation. Because the proportion of the preparation in partially folded conformation is unknown, this increase must be considered a lower limit. Apparent increases in α-helix content were not significant at $p < 0.05$. These data suggest that the tau intermediate is a partially folded monomer enriched in β-sheet content relative to the starting conformation.

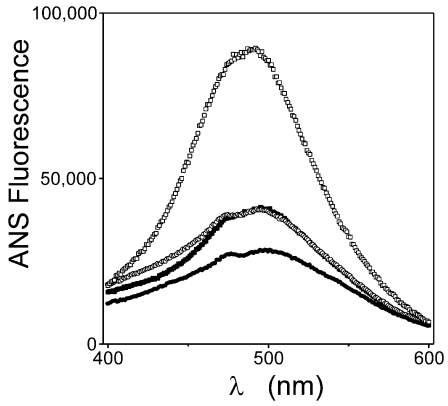

FIGURE 5: Effects of intermediate formation on ANS fluorescence spectra. Reactions containing assembly buffer and no additions (●), 1.9 μM htau40 (■), 1.9 μM htau40 and 50 μM AA inducer (□), or 0.8 μM protamine and 50 μM AA inducer (○) were prepared. After incubation (24 h at 25 °C), aliquots were removed, treated with 20 μM ANS (final concentration), and immediately subjected to fluorescence spectroscopy (λ_{ex} = 350 nm; λ_{em} = 400−600 nm). ANS in buffer alone fluoresced weakly at the optimum wavelength of λ_{em} = 500 nm (●). In contrast, intermediates prepared by incubation of htau40 with AA inducer fluoresced brightly with a blue-shifted optimum of λ_{em} = 487 nm (□). Neither tau without inducer (■) nor AA micelles formed in the presence of protamine (○) were capable of recapitulating the ANS fluorescence enhancement observed in the presence of htau40 with AA inducer, indicating that ANS binds preferentially to tau intermediates.

Intermediate Tertiary Structure. In addition to its secondary structure signature, the premolten globule state is characterized by a partially collapsed structure with a loosely packed hydrophobic core. To confirm that the intermediate had partially folded character, htau40 was incubated in the presence or absence of arachidonic acid inducer for 24 h and then examined for an ability to bind ANS, a fluorescent probe of surface-exposed hydrophobic patches (*39*−*41*). The analysis was conducted below the critical concentration to ensure that filaments did not contribute to ANS fluorescence. ANS in buffer alone fluoresced weakly at an optimum wavelength of λ_{em} = 500 nm. In contrast, ANS in the presence of intermediates (prepared by incubation of htau40 with AA inducer) fluoresced brightly with a blue-shifted optimum of λ_{em} = 487 nm (Figure 5). The increase in fluorescence intensity was not fully recapitulated by either tau protein alone or by AA micelles formed from incubation with protamine, indicating that the enhanced fluorescent signal observed in the presence of tau and AA came primarily from binding to altered conformations of tau (Figure 5). Taken together, the above data suggest that anionic inducers stabilize monomeric tau in a partially folded, β-sheet-enriched conformation and that this conformation precedes the polymerization reaction.

Intermediate Stabilization Triggers Tau Fibrillization. We hypothesize that formation of the intermediate conformation is necessary and sufficient for triggering fibrillization. If so, then conditions that stabilize the intermediate should induce tau fibrillization. To test this prediction, htau40 was incubated with increasing concentrations of ThS, a dye that binds tightly ($K_D \sim 1$ μM) to the intermediate conformation (*5*, *9*). Other dyes known to interact with β-structure were investigated as well, including Congo Red (*42*) and thiazin red (*43*).

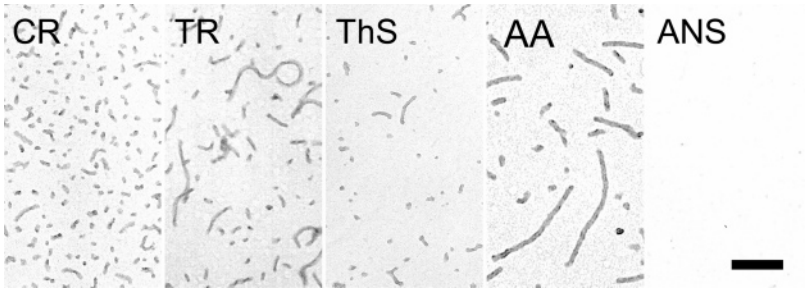

FIGURE 6: Planar aromatic dyes trigger tau fibrillization. Htau40 (4 μM) was incubated (24 h at 37 °C) under standard conditions with (from left to right) (A) 25 μM Congo Red (CR), (B) 100 μM thiazin red (TR), (C) 100 μM ThS, (D) 75 μM AA (3 h, 37 °C), or (E) 100 μM ANS. Planar aromatic dyes with known ability to bind β-sheet structure such as Congo Red, thiazin red, and ThS induced the formation of tau filaments with twisted ribbon morphology (see Figure 9 for higher magnification image) clearly distinct from the straight filaments induced by AA. In contrast, the aromatic dye ANS, which binds hydrophobic clusters in the partially folded intermediate, did not have inducer activity when tested in the range 5−500 μM. These data indicate that dyes complementary to β-sheet structure induce tau fibrillization and that the filament morphology observed reflects the fibrillization inducer employed. Bar = 100 nm.

Linkage theory (*44*) predicted that rising dye concentrations would drive tau monomer equilibrium toward the intermediate conformation by mass action and then toward the filamentous state through positive polysteric linkage with the self-association reaction (linkage refers to the influence of ligand binding upon other equilibria including aggregation reactions and phase transitions). Results confirmed that Congo Red, thiazin red, and ThS were all capable of inducing tau fibrillization independently of anionic inducers (Figure 6). Dye-induced filaments differed from anion-induced filaments in morphology, growing as twisted ribbons with maximum widths of 25 ± 4 nm, minimum widths of 11 ± 2 nm, and half periodicity of 170 ± 39 nm (n = 42) during time periods ≤24 h. In contrast, straight filaments formed over identical time periods with arachidonic acid had a consistent width of 13 ± 2 nm (n = 45) and no twist (Figure 6). Moreover, dye-induced filaments were greater in number and shorter in length than arachidonic acid induced filaments, suggesting that dyes were especially efficacious inducers of nucleation. Although capable of binding the partially folded structure of the intermediate, ANS did not induce fibrillization at concentrations up to 500 μM, indicating that the linkage reaction was selective for anionic planar aromatic dyes known to bind β-sheet structure (Figure 6). Congo Red was the most potent and efficacious inducer tested, with concentrations as low as 10 μM yielding large numbers of small filaments (Figure 6). ThS treatment also led to large numbers of small filaments, but its potency was at least 10-fold lower than Congo Red. Thiazin red was the least efficacious ligand tested, yielding few filaments of relatively long length at optimal concentrations. Nonetheless, these filaments were most amenable to experimentation (because they were fewer in number and longer in length), and so thiazin red was used for detailed characterization experiments described below.

To quantify the potency of the reaction, htau40 was incubated with varying concentrations of thiazin red and assayed for fibrillization using quantitative EM. Inducer activity followed a biphasic log-normal concentration response curve with an optimum potency of 114 ± 2 and 115 ± 3 μM in the presence of 1 and 2 μM htau40, respectively (Figure 7). Congo Red followed a similar profile, although the concentration optimum appeared ~10-fold lower (data not shown). These data indicate that, unlike anionic inducers, dye-mediated fibrillization reactions do not depend on tau/inducer ratios.

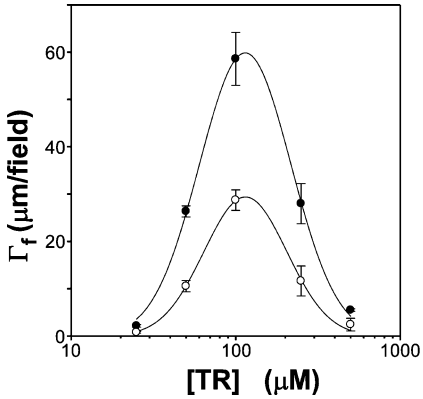

FIGURE 7: Potency of thiazin red dependent tau fibrillization. The dependence of the tau fibrillization equilibrium on thiazin red concentration (0−1000 μM) was determined in the presence of 1 (○) or 2 μM (●) htau40 after 24 h incubation at 37 °C by quantitative electron microscopy. Each data point represents the mean ± SD of triplicate determinations whereas the solid lines represent the best fit to a log-normal distribution (eq 3). The concentration response curves were biphasic, with an optimum centered on ~114 μM.

Intermediate Stabilization Promotes Filament Nucleation. To determine whether thiazin red influenced filament nucleation rates, the time course of htau40 fibrillization was followed by EM over a period of up to 24 h in the presence of 50 and 100 μM thiazin red at 37 °C and no agitation. When incubated at htau40 concentrations ≤1 μM, reaction progress curves were sigmoidal with clear lag, exponential growth, and equilibrium phases (Figure 8). As thiazin red concentrations were raised from 50 to 100 μM in the presence of 0.8 μM htau40, lag times decreased from 0.73 ± 0.09 h to 0.30 ± 0.04 h (Figure 8). These data suggest that acceleration of tau fibrillization with dye inducers results from increased rates of filament nucleation.

To confirm this observation, tau fibrillization induced by anionic microspheres was examined in the presence and absence of thiazin red. Nucleation events were counted as the number of filaments formed on the surface of each microsphere (Figure 9). In the absence of thiazin red ~80% of beads had no filaments, ~20% had one filament (Figure 9A), and a small percentage had two filaments (Figure 9C).

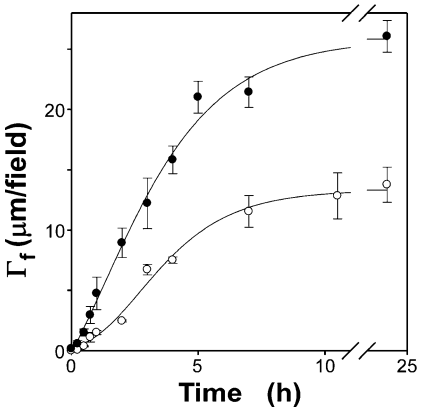

FIGURE 8: Thiazin red modulates tau nucleation rate. The time course (37 °C) of htau40 (0.8 μM) fibrillization in the presence of 50 (○) or 100 (●) μM thiazin red was determined by EM. Each data point represents total filament length/field (Γ_f) as a function of time whereas each sigmoid curve represents the best fit of the data points to a three-parameter Gompertz function. Lag times calculated as described in Experimental Procedures were 0.73 ± 0.09 and 0.30 ± 0.04 h for 50 and 100 μM thiazin red, respectively. The concentration dependence of the lag time was consistent with thiazin red increasing the rate of tau filament nucleation.

Beads with three or more filaments were never observed (n = 100). The data fit a Poisson distribution (averaging 0.19 filament/microsphere), indicating that nucleation events were random and independent of each other. Addition of thiazin red to 50 μM concentration shifted the Poisson distribution so that the average microsphere contained 1.95 filaments (Figure 9B,C). Further increase in thiazin red concentrations to 100 μM raised the average still higher to 2.17 filaments/microsphere. Together, these data suggest that intermediate stabilization had a large positive effect on nucleation rate and that the effect was additive with anionic inducers.

Effects of Intermediate Stabilization on Critical Concentration. In the presence of thiazin red, htau40 fibrillized at submicromolar concentration, far below the critical concentration estimated in the presence of anionic inducers. To clarify this issue, critical concentrations were estimated as a function of thiazin red concentration. Results showed extremely low critical concentrations of 0.20 ± 0.07 and 0.21 ± 0.05 at 50 and 100 μM thiazin red concentrations, respectively (Figure 10). These data indicate that thiazin red treatment led to critical concentrations 10-fold lower than did anionic inducers and that the presence of dyes influenced postnuclear equilibria in addition to nucleation rate and filament morphology.

Thiazin Red Induces Fibrillization in Monomeric Form. Although anionic inducers such as arachidonic acid are monomers below 200 μM in aqueous solution, the presence of protein such as tau triggers the rapid formation of micellar aggregates in which fibrillization-inducing activity resides (*16*). Planar aromatic dyes also self-assemble to form supramolecular aggregates at high concentration (*45*, *46*), suggesting that formation of anionic micelles may also mediate the dye inducer activity. To test this hypothesis, the absorbance properties of thiazin red were measured in the presence and absence of tau protein. Dye aggregation is accompanied by characteristic shifts in absorbance optima depending on the structure of the aggregate formed (*47*). In methanol, where dye aggregation is not supported, thiazin red absorbance was characterized by a major peak centered

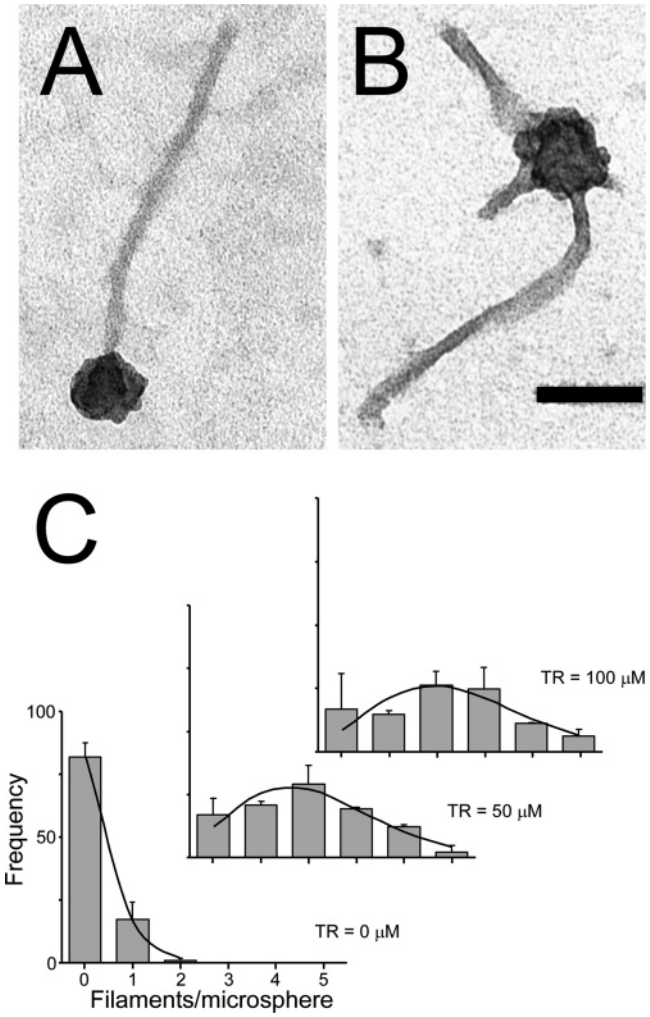

FIGURE 9: Thiazin red increases frequency of heterogeneous nucleation. Carboxylate-substituted polystyrene microspheres (90 nm diameter, 11.6 Å^2/eq molecular area; 124 pM) were incubated (24 h at 37 °C) with htau40 (4 μM) in the (A) absence or (B) presence of 50 μM thiazin red and then visualized by transmission EM. In the absence of thiazin red, microspheres induced the formation of straight filaments, with frequency rarely exceeding one nucleation event per bead. In contrast, the presence of thiazin red increased nucleation frequency so that multiple filaments per bead were a common occurrence. Note the change in filament morphology to twisted ribbon in the presence of thiazin red. (C) Statistical distributions of the number of nucleation events per bead were then calculated for reactions conducted in the presence of 0, 50, and 100 μM thiazin red (TR). Each bar represents the number of nucleations (filaments) per bead normalized as percent frequency, whereas each solid line represents the best fit of the data to the Poisson distribution (eq 4). Thiazin red increased nucleation frequency so that more multiple filaments per bead were observed. Bar = 100 nm.

at 514 nm and a shoulder at 548 nm (Figure 11). This pattern is characteristic of hydrazone tautomers of 1-naphthol-2-phenylazo derivatives such as thiazin red (*48*−*50*). The pattern did not change significantly in the presence of aqueous buffer with or without tau protein (Figure 11). These data suggest that thiazin red does not form detectable supramolecular complexes under assay conditions and that the active form of the dye is a planar monomer.

DISCUSSION

Triggers of Tau Fibrillization. Isolated tau proteins have the hydrodynamic properties of random coil monomers in

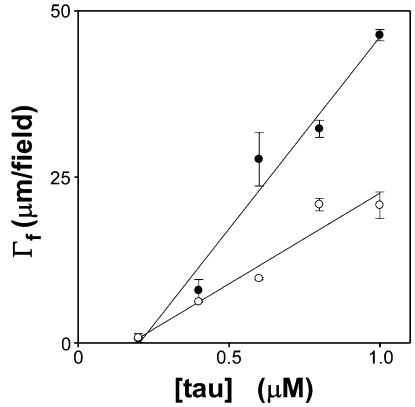

FIGURE 10: Critical concentration of tau fibrillization in the presence of thiazin red. The dependence of fibrillization equilibrium on tau concentration (0.1−2 μM) was determined in the presence of 50 (○) or 100 μM (●) thiazin red after 24 h incubation at 37 °C by quantitative electron microscopy. Each data point represents the mean ± SD of triplicate determinations whereas the solid lines represent the best fit to a linear regression. Critical concentrations determined from the intercepts of regression lines with the abscissa were 0.20 ± 0.07 and 0.21 ± 0.05 at 50 and 100 μM thiazin red concentrations, respectively.

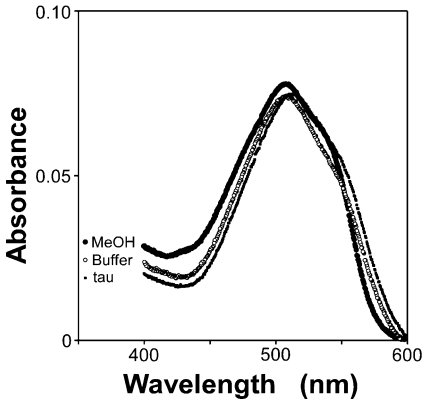

FIGURE 11: Thiazin red induces tau fibrillization in monomeric form. Thiazin red was dissolved in either methanol (●), assembly buffer (○), or assembly buffer containing 4 μM htau40 (■), incubated for 24 h at 37 °C, and finally subjected to absorbance scans in the range of 400−600 nm. All curves showed an absorbance maximum centered on 514 nm with a shoulder at 548 nm, suggesting that thiazin red did not aggregate into supermolecular complexes under standard assay conditions.

solution, consistent with their equilibrium conformation being "natively unfolded". Despite the lack of organized tertiary structure, tau monomers do not assemble spontaneously under physiological conditions over experimentally tractable time periods. The barrier to aggregation can be overcome in vitro through truncation of the tau molecule to short peptides within the microtubule-binding repeat region (the region that mediates fibrillization in vivo). Indeed, peptide fragments ranging from as small as two amino acids (*51*) to as large as four full repeats (*52*−*54*) aggregate spontaneously to form amyloid filaments over a period of days when incubated at high concentration (>150 μM). Spontaneous assembly becomes progressively less efficient as the length of tau increases toward full-length isoforms (*52*), eventually requiring extremes of ionic strength, pH, temperature, and tau concentrations (*8*). At near-physiological buffer conditions and tau concentrations (1−10 μM; ref *5*), aggregation of full-length isoforms becomes still less favorable and virtually undetectable over a period of weeks (*9*). These data suggest that the rate-limiting barrier for aggregation of full-length tau isoforms is conformational in nature.

Although truncation reduces the conformational barrier to aggregation, the macroscopic pathway observed in authentic tissue indicates that the initial steps of aggregation involve primarily full-length tau isoforms (*13*). What triggers fibrillization of full-length tau under physiological conditions? In the case of anionic inducers it appears to be the stabilization of monomeric intermediates characterized by increased β-structure (as detected by circular dichroism and binding of fluorescent probe ThS) and partially collapsed tertiary structure (as detected by fluorescent probe ANS) resembling a premolten globule state. Similar states mediate the fibrillization of α-synuclein and amylin (*55*−*57*), suggesting commonality in the mechanism of fibrillization of natively unfolded proteins. However, not all intermediates may be thioflavin dye reactive, and not all reactive intermediates are monomers. For example, aggregation of transthyretin monomer initiated by shifting supersaturated solutions to acidic pH yields immediate formation of thioflavin dye reactivity as found here for tau protein (*58*). In the case of transthyretin, however, thioflavin dye reactivity appeared in tandem with protein oligomers rather than monomers. Consistent with the reactive species being multimeric, the initial velocity of thioflavin dye fluorescence increased as a power function of protein concentration (Figure 1D, ref *58*). These data indicate that the intermediates involved in amyloid formation may be structurally diverse.

In the current work, tau assembly intermediates appeared in the presence of anionic surfactants and microspheres, but it is likely that other tau fibrillization inducers act similarly. For example, treatment of tau with the polyanion inducer heparin modulates its ability to serve as a substrate for protein kinases, indicating a change in conformation upon binding (*59*). In addition, solvent additives such as urea that induce fibrillization of full-length tau proteins (*60*, *61*) also modulate the formation of assembly-competent conformations of insulin (*62*). In both cases, activity resides with urea but not guanidine. Together, these data are consistent with the stabilization of assembly-competent intermediate conformations being intimately connected with the triggering of fibrillization.

The conversion from natively unfolded tau to the assembly-competent intermediate has the characteristics of an allosteric transition. Initially, natively unfolded htau40 is an extended monomer containing ~25% of residues in β-strand conformation. In the presence of anionic surfactant inducer, htau40 adopts a condensed conformation containing additional β-conformation. In addition to anionic surfactants, tau fibrillization can be induced by planar anionic aromatic ligands complementary to β-sheet structure such as Congo Red, thiazin red, and ThS. In contrast, the nonplanar anionic aromatic dye ANS, which has affinity for condensed folding states including premolten globule but not for β-sheet structure (*63*), did not induce tau fibrillization even at concentrations up to 500 μM. These data suggest that the formation of additional β-sheet structure in the intermediate is a key requirement for triggering the nucleation reaction. It cannot be excluded, however, that certain structural elements interfere with nucleation and are resolved by intermediate formation.

The Tau Aggregation Pathway. Once β-sheet-enriched intermediates are populated, tau aggregates spontaneously in a reaction characterized by a lag time and critical concentration. In terms of aggregation kinetics, intermediate formation leads to shorter aggregation lag times reflecting increased rates of nucleation. Because intermediate formation is rapid and intramolecular, oligomerization (including dimer formation) appears to be a secondary reaction potentially related to nucleation.

How does intermediate stabilization promote filament nucleation? Hypothetical models of amyloid fibrils constructed from fiber diffraction patterns provide potential clues. Intramolecular refolding models (*64*), where amino acid residues of a single protein protomer form parallel and cylindrical β-sheets, are consistent with monomeric nucleus cluster sizes determined from nucleation rates (*65*). In this case, the rate-limiting intramolecular conformational change is necessary and sufficient for the elongation reaction to proceed spontaneously. In other words, intramolecular refolding is coincident with the nucleation reaction. In contrast, the intermolecular association of β-sheets predicted by zipper-spine models (*66*) suggests that nucleation of this structure involves protein oligomerization to form a stable unit cell before elongation is supported. Because the tau nucleus is oligomeric (*10*), tau filaments are better modeled by the zipper-spine model than the intramolecular-folding model put forth for proteins containing poly(L-glutamine) tracts. We propose that tau nucleation corresponds to an oligomerization reaction involving face-to-face packing of β-sheet segments arranged orthogonal to the fiber axis (*66*, *67*). Seen in this way, one major role of intermediate formation is to prearrange β-sheet structure for incorporation into the oligomeric nucleus. Once nucleated, the nascent filament lengthens by addition of protomers parallel to the filament axis. Filaments synthesized from recombinant htau34 containing the P301S mutation attain a final β-sheet content of 57 ± 6% (*3*). This value suggests that β-structure extends far beyond the ~90 amino acid residue core of paired helical filaments (*68*). These data are consistent with the progression from natively unfolded full-length monomer to intermediate and finally filament conformation being characterized by continuously increasing β-sheet content.

In vitro, tau filament morphology varies with isoform (*69*) and primary structure (*54*). The data presented herein indicates that morphology also depends on the nature of the inducer. Anionic surfactants and microspheres induce primarily untwisted 13 nm wide filaments from htau40 over early time periods, and these transition to twisted filaments with the mass per unit length of paired helical filaments over a period of days (*70*). In contrast, thiazin red induced twisted ribbons with a maximal width of 25 nm from the earliest time points. The factors influencing amyloid filament morphology are not fully understood. In the cases of β2-microglobulin (*71*) and the immunoglobulin light chain variable domain (*72*), filament morphology is linked to the conformational properties of the precursor state. Differences tau filament morphology in the presence of different inducers may reflect similar considerations. In fact, it is conceivable that nucleation rate, filament morphology, and critical concentration all depend on the nature of the fibrillization inducer owing in part to differences in the fine structures of the intermediate species they stabilize. Alternatively, dyes may incorporate into filaments and thereby influence morphology at other stages of assembly. Because tau filaments develop over a period of decades (*73*), the final conformation of filaments in vivo (i.e., paired helical filaments) may reflect free energy considerations (*74*) rather than just the nature of the inducer or structure of the assembly intermediate.

Triggers and Enhancers. What triggers fibrillization of full-length tau isoforms in sporadic disease? The endwise association of tau filaments with intracellular membranes in biopsy specimens of AD tissue (*14*) suggests that anionic surfaces may present pathophysiologically relevant sources of triggering activity. But as shown here, planar aromatic dyes also can trigger the fibrillization reaction, perhaps mimicking the activity of naturally occurring small molecules (*75*). Indeed, small-molecule metabolites can induce the fibrillization of proteins other than tau (*76*), suggesting additional sources of exogenous triggering activity. Moreover, tissue-derived tau contains multiple posttranslational modifications, and these too may trigger the aggregation reaction. For example, phospho-tau isolated from AD brain aggregates spontaneously in vitro in a reaction that is antagonized by phosphatase treatment (*77*). However, these experiments require pretreatment of tau with urea, a known modulator of intermediate structure (*62*). In fact, both phosphorylation mimicry and glycation enhance tau fibrillization at the step of elongation (*11*). Acting in this way, enhancers stabilize filaments and increase the driving force for nucleation without necessarily triggering the reaction. In terms of the zipper-spine model, triggers and enhancers are predicted to differentially affect the equilibria orthogonal and parallel to the filament axis, respectively. It is likely, therefore, that alternative splicing, mutation, and posttranslational modifications will have differential effects on the nucleation and extension phases of the tau aggregation reaction. It will be useful to characterize these modulators at the level of intermediate formation.

Pharmacological Considerations. Tau filament formation is a robust marker of degeneration and, so, is an attractive target for premortem diagnostic development. Small-molecule ligands capable of binding amyloid conformation with high affinity may be useful for this purpose (*78*). The data presented here, however, suggest that reagents such as these must be used with care owing to their ability to drive the fibrillization reaction. The high concentrations (>25 μM) required for dyes such as ThS to drive fibrillization suggest the existence of a preequilibrium, where binding to natively unfolded tau is slow because few binding sites are prearranged. It will be important to determine whether binding affinity for filaments can be separated from affinity for intermediate states or whether linkage with the nucleation reaction can be severed.

Conclusions. Protein aggregation is controlled by both conformational and colloidal stability in solution, either of which can be rate limiting for amyloid formation depending on conditions (*79*). Despite being natively unfolded, similar considerations apply to tau protein. Under physiological conditions, the equilibrium conformation of full-length htau40 is not assembly competent, and so the fibrillization reaction is triggered by those agents or mutations that stabilize assembly-competent conformations. Triggering activity is characterized by greatly accelerated nucleation rates. In contrast, posttranslational modifications that stabilize

the filamentous state by promoting the elongation reaction act as enhancers. These are characterized by decreases in critical concentration without acceleration of the nucleation reaction. Evolving models of amyloid structure suggest a physical basis to these observations.

ACKNOWLEDGMENT

We thank The Ohio State University scientists Mike Zhu, Center for Molecular Neurobiology, Gordon Renkes, Campus Chemical Instrumentation Center, and Erich Grotewold, Department of Plant Cellular and Molecular Biology, for assistance with fluorescence, CD, and absorption spectroscopy, respectively.

REFERENCES

1. Buee, L., Bussiere, T., Buee-Scherrer, V., Delacourte, A., and Hof, P. R. (2000) Tau protein isoforms, phosphorylation and role in neurodegenerative disorders, *Brain Res. Brain Res. Rev. 33*, 95−130.
2. Cleveland, D. W., Hwo, S. Y., and Kirschner, M. W. (1977) Physical and chemical properties of purified tau factor and the role of tau in microtubule assembly, *J. Mol. Biol. 116*, 227−247.
3. Berriman, J., Serpell, L. C., Oberg, K. A., Fink, A. L., Goedert, M., and Crowther, R. A. (2003) Tau filaments from human brain and from in vitro assembly of recombinant protein show cross-beta structure, *Proc. Natl. Acad. Sci. U.S.A. 100*, 9034−9038.
4. Necula, M., and Kuret, J. (2004) A static laser light scattering assay for surfactant-induced tau fibrillization, *Anal. Biochem. 333*, 205−215.
5. Chirita, C. N., and Kuret, J. (2004) Evidence for an intermediate in tau filament formation, *Biochemistry 43*, 1704−1714.
6. Ferrone, F. (1999) Analysis of protein aggregation kinetics, *Methods Enzymol. 309*, 256−274.
7. Friedhoff, P., Schneider, A., Mandelkow, E. M., and Mandelkow, E. (1998) Rapid assembly of Alzheimer-like paired helical filaments from microtubule-associated protein tau monitored by fluorescence in solution, *Biochemistry 37*, 10223−10230.
8. Crowther, R. A., Olesen, O. F., Smith, M. J., Jakes, R., and Goedert, M. (1994) Assembly of Alzheimer-like filaments from full-length tau protein, *FEBS Lett. 337*, 135−138.
9. King, M. E., Ahuja, V., Binder, L. I., and Kuret, J. (1999) Ligand-dependent tau filament formation: implications for Alzheimer's disease progression, *Biochemistry 38*, 14851−14859.
10. Friedhoff, P., von Bergen, M., Mandelkow, E. M., Davies, P., and Mandelkow, E. (1998) A nucleated assembly mechanism of Alzheimer paired helical filaments, *Proc. Natl. Acad. Sci. U.S.A. 95*, 15712−15717.
11. Necula, M., and Kuret, J. (2004) Pseudophosphorylation and glycation of tau protein enhance but do not trigger fibrillization in vitro, *J. Biol. Chem. 279*, 49694−49703.
12. Barghorn, S., and Mandelkow, E. (2002) Toward a unified scheme for the aggregation of tau into Alzheimer paired helical filaments, *Biochemistry 41*, 14885−14896.
13. Horowitz, P. M., Patterson, K. R., Guillozet-Bongaarts, A. L., Reynolds, M. R., Carroll, C. A., Weintraub, S. T., Bennett, D. A., Cryns, V. L., Berry, R. W., and Binder, L. I. (2004) Early N-terminal changes and caspase-6 cleavage of tau in Alzheimer's disease, *J. Neurosci. 24*, 7895−7902.
14. Gray, E. G., Paula-Barbosa, M., and Roher, A. (1987) Alzheimer's disease: paired helical filaments and cytomembranes, *Neuropathol. Appl. Neurobiol. 13*, 91−110.
15. Perez, M., Valpuesta, J. M., Medina, M., Montejo de Garcini, E., and Avila, J. (1996) Polymerization of tau into filaments in the presence of heparin: the minimal sequence required for tau-tau interaction, *J. Neurochem. 67*, 1183−1190.
16. Chirita, C. N., Necula, M., and Kuret, J. (2003) Anionic micelles and vesicles induce tau fibrillization in vitro, *J. Biol. Chem. 278*, 25644−25650.
17. Carmel, G., Mager, E. M., Binder, L. I., and Kuret, J. (1996) The structural basis of monoclonal antibody Alz50's selectivity for Alzheimer's disease pathology, *J. Biol. Chem. 271*, 32789−32795.
18. Necula, M., Chirita, C. N., and Kuret, J. (2003) Rapid anionic micelle-mediated alpha-synuclein fibrillization in vitro, *J. Biol. Chem. 278*, 46674−46680.
19. Schmid, F. X. (1997) Optical spectroscopy to characterize protein conformation and conformational changes, in *Protein Structure: A Practical Approach* (Creighton, T. E., Ed.) pp 261−297, IRL Press, Oxford.
20. Woody, R. W. (1996) Theory of circular dichroism of proteins, in *Circular Dichroism and the Conformational Analysis of Biomolecules* (Fasman, G. D., Ed.) pp 25−68, Plenum Press, New York.
21. Provencher, S. W., and Glockner, J. (1981) Estimation of globular protein secondary structure from circular dichroism, *Biochemistry 20*, 33−37.
22. Johnson, W. C. (1999) Analyzing protein circular dichroism spectra for accurate secondary structures, *Proteins 35*, 307−312.
23. Sreerama, N., Venyaminov, S. Y., and Woody, R. W. (1999) Estimation of the number of alpha-helical and beta-strand segments in proteins using circular dichroism spectroscopy, *Protein Sci. 8*, 370−380.
24. Sreerama, N., and Woody, R. W. (2000) Estimation of protein secondary structure from circular dichroism spectra: comparison of CONTIN, SELCON, and CDSSTR methods with an expanded reference set, *Anal. Biochem. 287*, 252−260.
25. Potschka, M. (1987) Universal calibration of gel permeation chromatography and determination of molecular shape in solution, *Anal. Biochem. 162*, 47−64.
26. Vancura, A., O'Connor, A., Patterson, S. D., Mirza, U., Chait, B. T., and Kuret, J. (1993) Isolation and properties of YCK2, a *Saccharomyces cerevisiae* homolog of casein kinase-1, *Arch. Biochem. Biophys. 305*, 47−53.
27. Siegel, L. M., and Monty, K. J. (1966) Determination of molecular weights and frictional ratios of proteins in impure systems by use of gel filtration and density gradient centrifugation. Application to crude preparations of sulfite and hydroxylamine reductases, *Biochim. Biophys. Acta 112*, 346−362.
28. Perkins, S. J. (1986) Protein volumes and hydration effects. The calculations of partial specific volumes, neutron scattering match-points and 280-nm absorption coefficients for proteins and glycoproteins from amino acid sequences, *Eur. J. Biochem. 157*, 169−180.
29. Tcherkasskaya, O., Davidson, E. A., and Uversky, V. N. (2003) Biophysical constraints for protein structure prediction, *J. Proteome Res. 2*, 37−42.
30. Evans, K. C., Berger, E. P., Cho, C. G., Weisgraber, K. H., and Lansbury, P. T., Jr. (1995) Apolipoprotein E is a kinetic but not a thermodynamic inhibitor of amyloid formation: implications for the pathogenesis and treatment of Alzheimer disease, *Proc. Natl. Acad. Sci. U.S.A. 92*, 763−767.
31. Philo, R. D., and Selwyn, M. J. (1973) Use of progress curves to investigate product inhibition in enzyme-catalysed reactions. Application to the soluble mitochondrial adenosine triphosphatase, *Biochem. J. 135*, 525−530.
32. Yao, T. M., Tomoo, K., Ishida, T., Hasegawa, H., Sasaki, M., and Taniguchi, T. (2003) Aggregation analysis of the microtubule binding domain in tau protein by spectroscopic methods, *J. Biochem. (Tokyo) 134*, 91−99.
33. Paudel, H. K. (1997) Phosphorylation by neuronal cdc2-like protein kinase promotes dimerization of Tau protein in vitro, *J. Biol. Chem. 272*, 28328−28334.
34. Zhao, D., and Moore, J. S. (2003) Nucleation-elongation: a mechanism for cooperative supramolecular polymerization, *Org. Biomol. Chem. 1*, 3471−3491.
35. Timasheff, S. N. (1981) The self-assembly of long rodlike structures, in *Protein−Protein Interactions* (Nichol, L. W., Ed.) pp 315−336, John Wiley and Sons, New York.
36. Fitzkee, N. C., and Rose, G. D. (2004) Reassessing random-coil statistics in unfolded proteins, *Proc. Natl. Acad. Sci. U.S.A. 101*, 12497−12502.
37. Uversky, V. N., and Fink, A. L. (2004) Conformational constraints for amyloid fibrillation: the importance of being unfolded, *Biochim. Biophys. Acta 1698*, 131−153.
38. Ruben, G. C., Ciardelli, T. L., Grundke-Iqbal, I., and Iqbal, K. (1997) Alzheimer disease hyperphosphorylated tau aggregates hydrophobically, *Synapse 27*, 208−229.
39. Semisotnov, G. V., Rodionova, N. A., Razgulyaev, O. I., Uversky, V. N., Gripas, A. F., and Gilmanshin, R. I. (1991) Study of the "molten globule" intermediate state in protein folding by a hydrophobic fluorescent probe, *Biopolymers 31*, 119−128.
40. Chaffotte, A. F., Guijarro, J. I., Guillou, Y., Delepierre, M., and Goldberg, M. E. (1997) The "pre-molten globule," a new intermediate in protein folding, *J. Protein Chem. 16*, 433−439.

41. Schonbrunn, E., Eschenburg, S., Luger, K., Kabsch, W., and Amrhein, N. (2000) Structural basis for the interaction of the fluorescence probe 8-anilino-1-naphthalene sulfonate (ANS) with the antibiotic target MurA, *Proc. Natl. Acad. Sci. U.S.A. 97*, 6345−6349.
42. Klunk, W. E., Pettegrew, J. W., and Abraham, D. J. (1989) Two simple methods for quantifying low-affinity dye-substrate binding, *J. Histochem. Cytochem. 37*, 1293−1297.
43. Mena, R., Edwards, P., Perez-Olvera, O., and Wischik, C. M. (1995) Monitoring pathological assembly of tau and beta-amyloid proteins in Alzheimer's disease, *Acta Neuropathol. (Berlin) 89*, 50−56.
44. Wyman, J., and Gill, S. J. (1990) *Binding and Linkage: Functional Chemistry of Biological Macromolecules*, University Science Books, Mill Valley, CA.
45. Stopa, B., Piekarska, B., Konieczny, L., Rybarska, J., Spolnik, P., Zemanek, G., Roterman, I., and Krol, M. (2003) The structure and protein binding of amyloid-specific dye reagents, *Acta Biochim. Pol. 50*, 1213−1227.
46. Stopa, B., Gorny, M., Konieczny, L., Piekarska, B., Rybarska, J., Skowronek, M., and Roterman, I. (1998) Supramolecular ligands: monomer structure and protein ligation capability, *Biochimie 80*, 963−968.
47. Murakami, K. (2002) Thermodynamic and kinetic aspects of self-association of dyes in aqueous solution, *Dyes Pigm. 53*, 31−43.
48. Antonov, L., and Stoyanov, S. (1995) Azo-quinonehydrazone tautomerism in 2-phenylazo-1-naphthol, *Dyes Pigm. 28*, 31−39.
49. Antonov, L., Gergov, G., Petrov, V., Kubista, M., and Nygren, J. (1999) UV−vis spectroscopic and chemometric study on the aggregation of ionic dyes in water, *Talanta 49*, 99−106.
50. Iijima, T., Jojima, E., Antonov, L., Stoyanov, S., and Stoyanova, T. (1998) Aggregation and tautomeric properties of CI Acid Red 138, *Dyes Pigm. 37*, 81−92.
51. Goux, W. J., Kopplin, L., Nguyen, A. D., Leak, K., Rutkofsky, M., Shanmuganandam, V. D., Sharma, D., Inouye, H., and Kirschner, D. A. (2004) The formation of straight and twisted filaments from short tau peptides, *J. Biol. Chem. 279*, 26868−26875.
52. Schweers, O., Mandelkow, E. M., Biernat, J., and Mandelkow, E. (1995) Oxidation of cysteine-322 in the repeat domain of microtubule-associated protein tau controls the in vitro assembly of paired helical filaments, *Proc. Natl. Acad. Sci. U.S.A. 92*, 8463−8467.
53. Arrasate, M., Perez, M., Armas-Portela, R., and Avila, J. (1999) Polymerization of tau peptides into fibrillar structures. The effect of FTDP-17 mutations, *FEBS Lett. 446*, 199−202.
54. Perez, M., Arrasate, M., Montejo De Garcini, E., Munoz, V., and Avila, J. (2001) In vitro assembly of tau protein: mapping the regions involved in filament formation, *Biochemistry 40*, 5983−5991.
55. Kayed, R., Bernhagen, J., Greenfield, N., Sweimeh, K., Brunner, H., Voelter, W., and Kapurniotu, A. (1999) Conformational transitions of islet amyloid polypeptide (IAPP) in amyloid formation in vitro, *J. Mol. Biol. 287*, 781−796.
56. Uversky, V. N., Li, J., and Fink, A. L. (2001) Evidence for a partially folded intermediate in α-synuclein fibril formation, *J. Biol. Chem. 276*, 10737−10744.
57. Uversky, V. N., Lee, H. J., Li, J., Fink, A. L., and Lee, S. J. (2001) Stabilization of partially folded conformation during α-synuclein oligomerization in both purified and cytosolic preparations, *J. Biol. Chem. 276*, 43495−43498.
58. Hurshman, A. R., White, J. T., Powers, E. T., and Kelly, J. W. (2004) Transthyretin aggregation under partially denaturing conditions is a downhill polymerization, *Biochemistry 43*, 7365−7381.
59. Paudel, H. K., and Li, W. (1999) Heparin-induced conformational change in microtubule-associated protein Tau as detected by chemical cross-linking and phosphopeptide mapping, *J. Biol. Chem. 274*, 8029−8038.
60. Montejo de Garcini, E., Carrascosa, J. L., Correas, I., Nieto, A., and Avila, J. (1988) Tau factor polymers are similar to paired helical filaments of Alzheimer's disease, *FEBS Lett. 236*, 150−154.
61. Montejo de Garcini, E., and Avila, J. (1987) In vitro conditions for the self-polymerization of the microtubule-associated protein, tau factor, *J. Biochem. (Tokyo) 102*, 1415−1421.
62. Ahmad, A., Millett, I. S., Doniach, S., Uversky, V. N., and Fink, A. L. (2004) Stimulation of insulin fibrillation by urea-induced intermediates, *J. Biol. Chem. 279*, 14999−15013.
63. Kamen, D. E., and Woody, R. W. (2001) A partially folded intermediate conformation is induced in pectate lyase C by the addition of 8-anilino-1-naphthalenesulfonate (ANS), *Protein Sci. 10*, 2123−2130.
64. Perutz, M. F., Finch, J. T., Berriman, J., and Lesk, A. (2002) Amyloid fibers are water-filled nanotubes, *Proc. Natl. Acad. Sci. U.S.A. 99*, 5591−5595.
65. Chen, S., Ferrone, F. A., and Wetzel, R. (2002) Huntington's disease age-of-onset linked to polyglutamine aggregation nucleation, *Proc. Natl. Acad. Sci. U.S.A. 99*, 11884−11889.
66. Ivanova, M. I., Sawaya, M. R., Gingery, M., Attinger, A., and Eisenberg, D. (2004) An amyloid-forming segment of beta2-microglobulin suggests a molecular model for the fibril, *Proc. Natl. Acad. Sci. U.S.A. 101*, 10584−10589.
67. Diaz-Avalos, R., Long, C., Fontano, E., Balbirnie, M., Grothe, R., Eisenberg, D., and Caspar, D. L. (2003) Cross-beta order and diversity in nanocrystals of an amyloid-forming peptide, *J. Mol. Biol. 330*, 1165−1175.
68. Novak, M., Kabat, J., and Wischik, C. M. (1993) Molecular characterization of the minimal protease resistant tau unit of the Alzheimer's disease paired helical filament, *EMBO J. 12*, 365−370.
69. Hasegawa, M., Crowther, R. A., Jakes, R., and Goedert, M. (1997) Alzheimer-like changes in microtubule-associated protein Tau induced by sulfated glycosaminoglycans. Inhibition of microtubule binding, stimulation of phosphorylation, and filament assembly depend on the degree of sulfation, *J. Biol. Chem. 272*, 33118−33124.
70. King, M. E., Ghoshal, N., Wall, J. S., Binder, L. I., and Ksiezak-Reding, H. (2001) Structural analysis of Pick's disease-derived and in vitro-assembled tau filaments, *Am. J. Pathol. 158*, 1481−1490.
71. Smith, D. P., Jones, S., Serpell, L. C., Sunde, M., and Radford, S. E. (2003) A systematic investigation into the effect of protein destabilisation on beta 2-microglobulin amyloid formation, *J. Mol. Biol. 330*, 943−954.
72. Khurana, R., Gillespie, J. R., Talapatra, A., Minert, L. J., Ionescu-Zanetti, C., Millett, I., and Fink, A. L. (2001) Partially folded intermediates as critical precursors of light chain amyloid fibrils and amorphous aggregates, *Biochemistry 40*, 3525−3535.
73. Morsch, R., Simon, W., and Coleman, P. D. (1999) Neurons may live for decades with neurofibrillary tangles, *J. Neuropathol. Exp. Neurol. 58*, 188−197.
74. Turner, M. S., Briehl, R. W., Ferrone, F. A., and Josephs, R. (2003) Twisted protein aggregates and disease: the stability of sickle hemoglobin fibers, *Phys. Rev. Lett. 90*, 128103.
75. Santa-Maria, I., Hernandez, F., Martin, C. P., Avila, J., and Moreno, F. J. (2004) Quinones facilitate the self-assembly of the phosphorylated tubulin binding region of tau into fibrillar polymers, *Biochemistry 43*, 2888−2897.
76. Zhang, Q., Powers, E. T., Nieva, J., Huff, M. E., Dendle, M. A., Bieschke, J., Glabe, C. G., Eschenmoser, A., Wentworth, P., Jr., Lerner, R. A., and Kelly, J. W. (2004) Metabolite-initiated protein misfolding may trigger Alzheimer's disease, *Proc. Natl. Acad. Sci. U.S.A. 101*, 4752−4757.
77. Alonso, A., Zaidi, T., Novak, M., Grundke-Iqbal, I., and Iqbal, K. (2001) Hyperphosphorylation induces self-assembly of tau into tangles of paired helical filaments/straight filaments, *Proc. Natl. Acad. Sci. U.S.A. 98*, 6923−6928.
78. Zhuang, Z. P., Kung, M. P., Wilson, A., Lee, C. W., Plossl, K., Hou, C., Holtzman, D. M., and Kung, H. F. (2003) Structure−activity relationship of imidazo[1,2-a]pyridines as ligands for detecting beta-amyloid plaques in the brain, *J. Med. Chem. 46*, 237−243.
79. Chi, E. Y., Krishnan, S., Kendrick, B. S., Chang, B. S., Carpenter, J. F., and Randolph, T. W. (2003) Roles of conformational stability and colloidal stability in the aggregation of recombinant human granulocyte colony-stimulating factor, *Protein Sci. 12*, 903−913.

BI0500123